Strong-field spectral interferometry using the carrier–envelope phase

2013 New J. Phys. 15 073031

(http://iopscience.iop.org/1367-2630/15/7/073031)

New Journal of Physics
The open access journal for physics

Strong-field spectral interferometry using the carrier–envelope phase

C Ott[1,6], M Schönwald[1], P Raith[1], A Kaldun[1], G Sansone[1,2], M Krüger[3], P Hommelhoff[3,4], Y Patil[1], Y Zhang[1], K Meyer[1], M Laux[1] and T Pfeifer[1,5,6]

[1] Max-Planck-Institut für Kernphysik, Saupfercheckweg 1, D-69117 Heidelberg, Germany
[2] National Laboratory for Ultrafast and Ultraintense Optical Science–CNR-INFM, Department of Physics, Politecnico di Milano, Piazza Leonardo da Vinci 32, I-20133 Milano, Italy
[3] Max-Planck-Institut für Quantenoptik, Hans-Kopfermann-Strasse 1, D-85748 Garching, Germany
[4] Department für Physik, Universität Erlangen-Nürnberg, Staudtstr. 1, D-91058 Erlangen, Germany
[5] Center for Quantum Dynamics, Ruprecht-Karls-Universität Heidelberg, D-69117 Heidelberg, Germany
E-mail: christian.ott@mpi-hd.mpg.de and tpfeifer@mpi-hd.mpg.de

New Journal of Physics **15** (2013) 073031 (15pp)
Received 11 April 2013
Published 16 July 2013
Online at http://www.njp.org/
doi:10.1088/1367-2630/15/7/073031

Abstract. The carrier–envelope phase (CEP) of ultrashort laser pulses is an important parameter in strong-field physics that controls temporally localized events on a sub-cycle timescale. The relative timing of these events is directly encoded into the measured spectral intensity distribution, and can be accessed by the use of spectral interferometry. Here, we combine this analysis with CEP control in a two-dimensional way, creating a novel spectroscopic method to explore the temporal dynamics of strong-field processes. We apply this general method to CEP-dependent high-harmonic generation and find that

[6] Authors to whom any correspondence should be addressed.

contributions of three different sub-cycle electron quantum paths can be separated, allowing one to quantify the dipole-phase dependence on the CEP in the non-adiabatic regime. The CEP-dependent time delay between two full-cycle spaced attosecond pulses was determined to modulate by 54 ± 16 as. We confirm the generality of the method by further applying it to CEP-dependent photoemission from a nanoscale metal tip.

Contents

1. Introduction

In strong few-cycle laser fields, the carrier–envelope phase (CEP), i.e. the phase difference between the optical carrier signal and the pulse envelope [1], is an important parameter as it allows one to steer electron wavepackets on their natural attosecond timescale [2]. In such experiments, the electron wavefunction typically follows several quantum trajectories or transition pathways that are locked to the shape of the driving electric field (e.g. ionization or recombination). The experimentally observed response is then the coherent sum over all these trajectories, which are typically separated by a half- or full-optical cycle of the laser field. The interference of multiple overlapping contributions shows up in the spectrum and generally prevents the observation of distinct trajectories or their quantum phases. A technique to separate and disentangle the individual temporally localized quantum-path contributions in the time domain has thus far been lacking.

For the special case of two interfering trajectories, an intuitive time-domain picture of the measured spectral intensity distribution was given in, e.g., [3, 4]. It has been demonstrated how the CEP can be set such that predominantly two photoelectron emission events occur within the laser pulse, leading to an attosecond double slit in time. Spectral interferometry (SI) [5, 6] is a powerful tool to analyze the temporal dynamics of two such interfering events. It is based on Fourier analysis, which extracts complex (both amplitude and phase) information from the periodic modulations of the measured spectral intensity distribution. The retrieved phase information then directly relates to the relative phase of the interfering temporal events.

Here we combine the method of CEP control with SI, which allows direct *in situ* and quantitative temporal access to strong-field electron dynamics. The resulting CEPSI data provide two-dimensional (2D) *temporal* information in a manner similar (although qualitatively

different) to the way in which 2D spectroscopy allows the extraction of otherwise inseparable *spectral* features [7, 8]. For a first demonstration, we will apply the CEPSI method to the example of high-order harmonic generation (HHG). We show how three interfering electron trajectories, creating an attosecond pulse train (APT) within the driving few-cycle pulse, can be qualitatively and quantitatively disentangled in their relative timing and phase. However, the method itself can be considered to be general for the study of any CEP-dependent interference phenomenon. We demonstrate this by applying CEPSI also to strong-field photoemission from a nanoscale metal tip.

In the following section 2, we will develop and describe the CEPSI method in detail, applying it to high-harmonic spectra generated from CEP-controlled few-cycle laser fields. In section 3, we apply our method to electron emission, demonstrating another example of its experimental applicability. We show that, here, CEPSI allows extraction of CEP-dependent emission-time differences and reveals the total absence of interference for certain phase settings.

2. High-order harmonic generation from few-cycle laser fields, a first demonstration of the carrier–envelope phase spectral interferometry method

For few-cycle pulses in HHG, APT production is strongly influenced by the CEP. In this regime, known as the non-adiabatic regime [9, 10], a qualitative interpretation of non-adiabatic APT spectral signatures due to interference of only a few attosecond pulses within one single few-cycle laser pulse was discussed [11, 12], however without direct access to the temporal phases and relative timings that define the created APTs as a function of the CEP. Here, we separate the relative-phase contributions of individual pulses in an APT by measuring its readily accessible photon-energy spectrum only.

2.1. Experimental results

In the experiment, we used few-cycle laser pulses at 760 nm central wavelength with a stable CEP. The pulses were generated in a commercial amplified laser system (manufacturer: 'Femtolasers'), spectrally broadened via self-phase modulation in a neon-filled hollow-core fiber (∼1.5 bar pressure) and further compressed using chirped mirrors. The pulse duration on the order of 7 fs was determined via an interferometric autocorrelation based on second-harmonic generation. The CEP was stabilized and set via an f-to-2f interferometer, a feedback loop and by controlling the amount of glass in the stretcher stage of the laser system. After focusing with an $f = 500$ mm spherical mirror, HHG was driven in an ∼3 mm long cell filled with neon gas at ∼100 mbar backing pressure. To preferentially phase match short trajectories, the gas cell was placed just after the laser focus [13]. The generated HHG light is transmitted through a pair of 200 nm thin zirconium metal foils to remove the fundamental light. The remaining coherent extreme ultraviolet (XUV) light is spectrally separated with a 100 nm period free standing Si_3N_4 transmission grating and detected with a back-illuminated x-ray CCD camera.

In figure 1, experimental spectra are shown for five selected values of the CEP, where φ_{CEP} is of course only known up to a constant offset. The spectra exhibit interference structures with the well-known $2\hbar\omega_0 \approx 3$ eV odd-harmonic spacing, with ω_0 being the laser fundamental frequency. For energies above ∼95 eV, the harmonics shift linearly from one order to the next within one CEP cycle, confirming earlier findings in the harmonic cutoff region [10, 14]. Interestingly, for certain CEPs, regions of low visibility contrast of the harmonic modulation

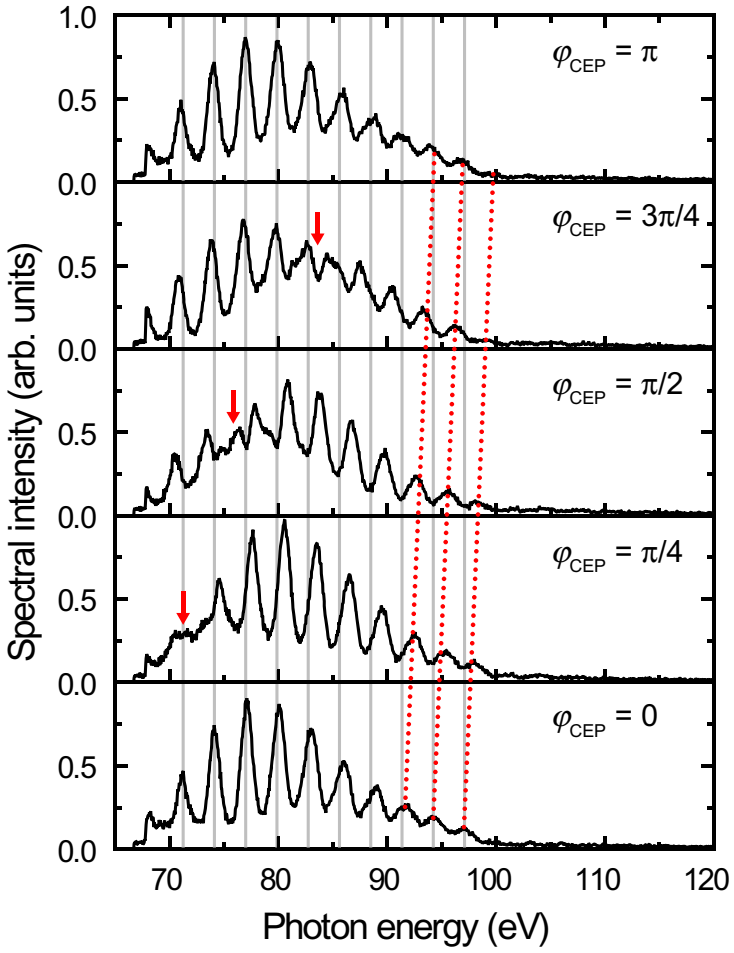

Figure 1. Experimentally obtained HHG spectra for various φ_{CEP}. The gray lines mark positions of constant photon energy, whereas the red dotted lines indicate the shifting of the high-energy harmonics as a guide to the eye. The region of low visibility contrast of high-harmonic peaks (marked with red arrows) is also observed moving through the spectrum as a function of φ_{CEP}.

appear in the spectral region below the cutoff (<95 eV). To analyze this behavior in more detail, a continuous scan of the CEP is carried out, which results in a 2D representation as shown in figure 2(a). The effect of a decreased contrast now shows up as a bifurcation-like switching between different harmonic peaks that rapidly sweeps through the spectra as a function of φ_{CEP}. Performing a Fourier analysis of the harmonic spectra and two-dimensionally plotting this for a continuous range of the CEP (figure 2(b)), in both amplitude (left panel) and phase (right panel), reveals characteristic features. In the Fourier-amplitude plot, the horizontal peak close to Fourier time $\tau \sim 1.4$ fs corresponds to temporal features separated by an optical half cycle. Local amplitude minima occur periodically at CEPs of 0.5π modulo π, yielding a double-peaked structure. The horizontal feature near Fourier time $\tau \sim 2.8$ fs corresponds to attosecond pulses temporally delayed by one full optical cycle. Only a faint contribution at ~4 fs (three optical half cycles) is visible, however an order of magnitude weaker than the other horizontal features, leading to the conclusion that a train of three most dominant attosecond pulses was produced. In addition, the Fourier phase shows significantly different CEP-dependent features

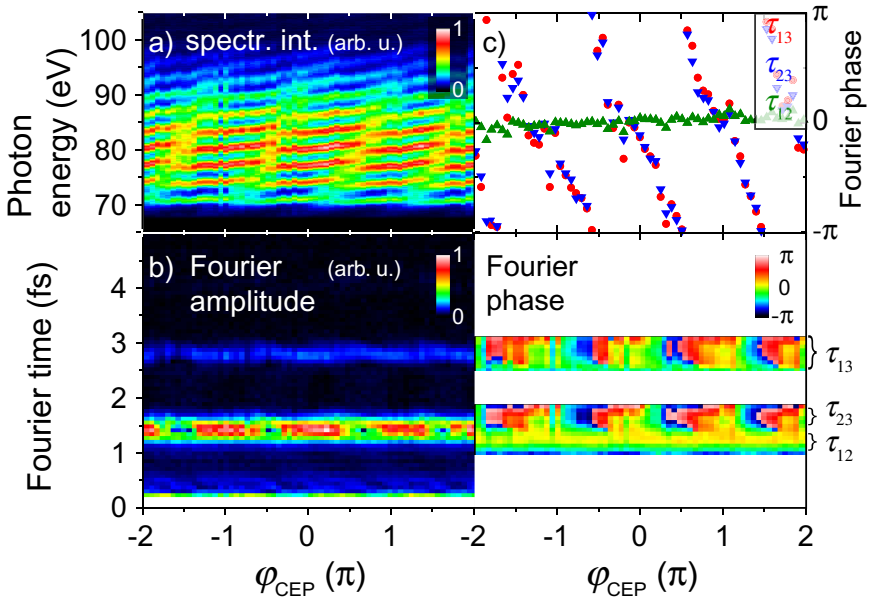

Figure 2. Experimental results: (a) high-harmonic spectrum recorded as a function of the CEP. At energies below 95 eV a splitting of the harmonics occurs at CEPs $\sim 0.5\pi$ modulo π. (b) Fourier analysis of (a): across the half-cycle Fourier peak at $\tau \sim 1.4$ fs a splitting of the amplitude as well as two distinct phase dependences are observed for smaller versus larger Fourier times, while the full-cycle Fourier peak at $\tau \sim 2.8$ fs is modulated in time and exhibits uniform phase behavior. The phase is only shown across the temporal region of interest with nonzero amplitude contribution. (c) The phase averaged over the marked temporal regions for τ_{12} (green triangle up), τ_{23} (blue triangle down) and $\tau_{13} = \tau_{12} + \tau_{23}$ (red circle) is shown to clarify the different CEP dependences of the Fourier phase.

when comparing the full-cycle and half-cycle peaks. The phase is fully modulated from $-\pi$ to π every $\Delta\varphi_{CEP} = \pi$ across the whole full-cycle peak, but only across the upper temporal part ($\tau > 1.4$ fs) of the half-cycle peak. In contrast, the lower temporal part of this peak ($\tau < 1.4$ fs) appears constant in phase as a function of the CEP. This difference is plotted in figure 2(c), where CEP-dependent lineouts are shown after temporally averaging the Fourier phase separately for the three different regions. The trivial temporal-phase oscillation related to the carrier frequency of the attosecond pulses was removed by shifting the spectrum close to zero frequency before the Fourier transformation. It is interesting to note that a Fourier-phase difference of π between the upper and lower temporal parts of the half-cycle peak appears coincident in the CEP where the Fourier amplitude exhibits the double-peaked behavior.

2.2. Theoretical toy model

In order to understand the origin of the above-described features, and to better illustrate the key point of CEPSI analysis, we first employ a simple 'toy model' of an APT (or in general, of temporally localized coherent events). In the time domain, it can be formally written as the

coherent sum of the electric fields of single attosecond pulses

$$A(t) = \sum_n A_n(t - t_n) \exp[\mathrm{i}\Phi_n(t - t_n)], \tag{1}$$

where $A_n(t)$ and $\Phi_n(t)$ are the amplitude and phase of each pulse, and t_n denotes their temporal position. In the spectral domain, interference structures (harmonics) will enter the intensity distribution whenever the slowly varying spectral amplitude functions $\tilde{A}_n(\omega)$ of different attosecond pulses share a common frequency range. Their spectral intensity modulation can be described as

$$S(\omega) \propto \sum_{m>n} \tilde{A}_n(\omega)\tilde{A}_m(\omega)\cos[\tilde{\Phi}_n(\omega) - \tilde{\Phi}_m(\omega) + \omega\tau_{nm}], \tag{2}$$

where $\tilde{\Phi}_n(\omega)$ is the frequency-dependent spectral phase of the nth pulse and $\tau_{nm} = t_m - t_n$ denotes their temporal difference. A Fourier transformation of equation (2) thus gives access to the individual interfering temporal contributions spaced by τ_{nm}. Problems with this SI method arise whenever multiple contributions are overlapping in their time delays τ_{nm}, as is the case for an APT with multiple half-cycle spaced ($\tau_{nm} = T/2$, where T is the optical cycle) attosecond pulses, and cannot be directly separated. However, using the CEP as an additional parameter, the separation can be performed. This is possible because in strong-field processes the CEP typically affects the phase of different temporal contributions (e.g. multiphoton transitions [15] or, here, recolliding electron trajectories) in a different way. In correspondence to the experimental observation, we now focus on the specific case of three attosecond pulses, each spaced by roughly half the optical cycle. However, CEPSI is not fundamentally limited to this number as it just relies on the varying influence of the CEP on each temporal event in the train.

To mimic the experimental results shown in figure 2, the temporal spacings $\tau_{12} = t_2 - t_1$ and $\tau_{23} = t_3 - t_2$ between the three pulses are chosen slightly asymmetrically ($\tau_{23} = \tau_{12} + \Delta$), where Δ is around 10% of τ_{12}. Slightly different temporal delays between the pulses are expected in the non-adiabatic regime [10], where the harmonic emission times (i.e. the electron recombination times for a given recombination energy) vary from half cycle to half cycle, which thus also affects the temporal spacing of consecutive attosecond pulses. This can be physically understood by just considering the short trajectory. For a given electron energy, recombination occurs significantly earlier in a more intense laser cycle as compared to a less intense laser cycle. The temporal phases $\Phi_{1,2}$ are chosen to be constant (CEP independent) for the first two pulses and to change by $\Phi_3 = 2\varphi_{\mathrm{CEP}}$ for the third pulse. The spectral interference pattern of such an asymmetric triple pulse is given in figure 3(a), two-dimensionally plotted as a function of φ_{CEP}. A Fourier transformation of these spectra is shown in figure 3(b), again in both amplitude (left) and phase (right). Now, the relative pulse characteristics, as previously set in this 'toy model', can be directly retrieved, which would not have been possible for a single value of the CEP or a CEP-averaged spectrum. The amplitude peak appearing at τ_{13} exhibits the linear phase difference of $2\varphi_{\mathrm{CEP}}$ between the two corresponding pulses. The amplitude peaks at τ_{12} and τ_{23} appear very close to each other and are thus difficult to separate. However, due to their different CEP dependence, separation is possible: an amplitude minimum appears in the temporal overlap region at $\varphi_{\mathrm{CEP}} = (n + 1/2)\pi$, i.e. when the relative phases between the first two and the latter two pulses are out of phase by π. The close agreement of this behavior with the experimental data presented in figure 2 suggests a similar dependence of the relative phases of the three attosecond pulses as a function of the CEP. Hence this interferometric analysis allows extraction of the CEP-dependent changes of the relative phases between the three pulses directly from the experimentally obtained harmonic spectra.

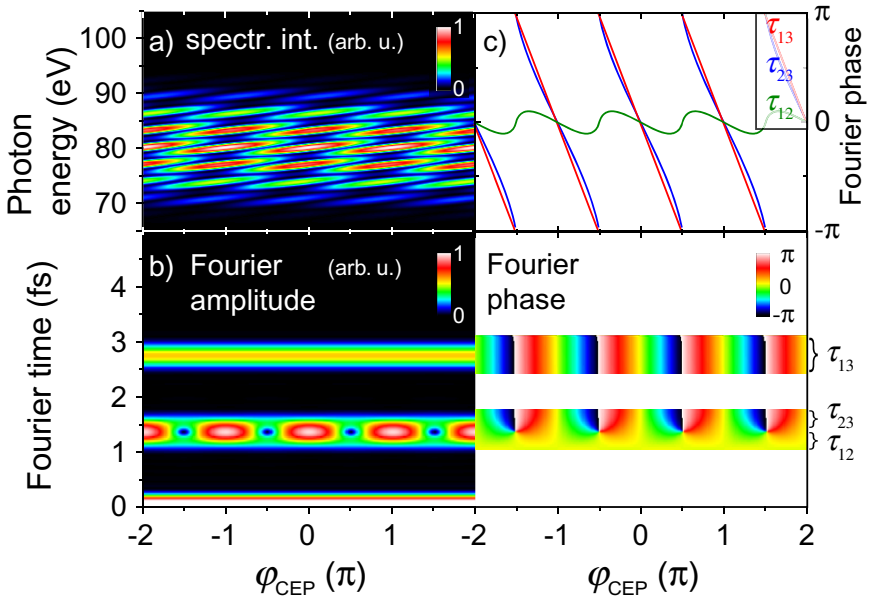

Figure 3. Spectral interference generated by a triple pulse with constant phases $\Phi_{1,2}$ and $\Phi_3 = 2\varphi_{CEP}$ and at non-equidistant temporal spacing $\tau_{23} \approx 1.1\tau_{12}$. (a) Spectra plotted as a function of φ_{CEP}. (b) Fourier analysis of (a) in both amplitude (left) and phase (right), where the correspondence to the different temporal components τ_{12}, τ_{23} and $\tau_{13} = \tau_{12} + \tau_{23}$ is indicated. (c) Fourier phase as a function of φ_{CEP} averaged over each temporal Fourier contribution as indicated in (b). Two otherwise temporally overlapping contributions ('temporally localized events') can thus be separated here by their CEP dependence in this 2D representation.

2.3. Quantum-mechanical model

To model the physical origin of the observed 'temporal triple slit', we carried out a simulation of HHG based on the strong-field approximation (SFA) and the quantum-mechanical three-step model [16, 17]. Only the short trajectories were considered. A 7 fs FWHM $\cos^2$-shaped laser pulse centered around 760 nm with peak electric field strength 0.10 au was used in the simulations (shown in figure 4(a)). For this proof-of-principle demonstration of the CEPSI method, we first neglect macroscopic effects and potentially non-Gaussian near-infrared (NIR) pulse shapes in the model. Comparing the simulated CEPSI spectra (figure 4(b)) with the experimental ones (figure 2(b)) reveals both qualitative and quantitative agreement. Note that the comparison in the Fourier-time domain allows us to extract and compare the essential features, the three most dominant *temporally localized* interfering pulses and their phases, which is not obvious from a comparison of the *broadband HHG spectra*.

The simulation results mapped with CEPSI now allow us to identify the origin of the observed triple-pulse dynamics, as shown in figure 4(c): the three most intense pulses exhibit a different temporal spacing at a given photon energy, indicated by the horizontal arrows τ_{12} and τ_{23}. Due to the different laser intensity of the corresponding half cycles, a photon energy around 85 eV corresponds to the half-cycle plateau region for the two most intense attosecond pulses and to the half-cycle cutoff region [18] for the third pulse, thus explaining the asymmetric

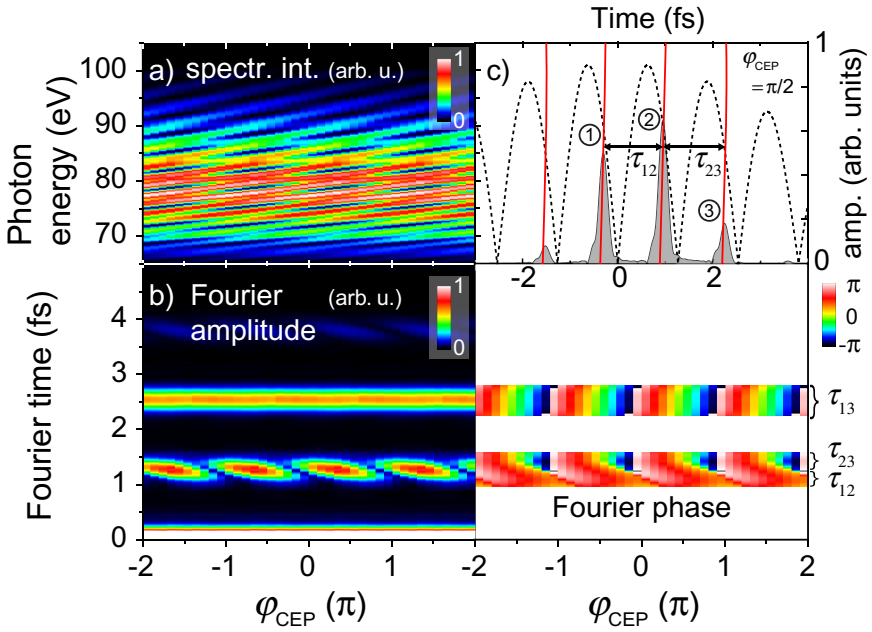

Figure 4. Strong-field (saddle-point) approximation simulation results: (a) spectral interference pattern as a function of the CEP. As in the experiment, below 90 eV, a splitting of harmonic positions at certain CEPs occurs. (b) Fourier analysis of (a) in both amplitude (left) and phase (right). Again, the qualitatively different phase contributions to the interferences of temporally localized events at τ_{12} and τ_{23} can be seen around 1.2 fs. (c) Short-trajectory photon energies (red solid line) for $\varphi_{CEP} = \pi/2$. The absolute values of the NIR electric field $|E(t)|$ (dashed line) and the attosecond pulse envelopes (gray shaded area) are also shown. The different temporal spacings τ_{12} and τ_{23} are indicated for the three most intense attosecond pulses in the energy region where the splitting effect occurs. The numbering of the pulses relates to the discussion in the text.

temporal spacing by the different sub-cycle intensity-dependent emission times for that photon energy. In the following, we extract the physical mechanism behind the different Fourier-phase dependences on the CEP. The Fourier phase encodes the relative phase of the interfering attosecond pulses. Therefore, changes of the relative phase between the attosecond pulses can be directly read out as a function of the CEP. The phase of the attosecond pulses is also known as the harmonic dipole phase [19]. Based on established theory [10, 19], the harmonic phase depends linearly on the laser intensity and on the time spent by the electron in the continuum. The variation of the phase with the intensity is thus more evident in the cutoff region due to the longer excursion time of the electron wavepacket, while it can be neglected for the plateau harmonics associated with the short trajectory. Here, by varying the CEP, we move individual attosecond pulse contributions up and down the envelope of the driver pulse [18], thus changing the local intensity at which they are produced on a sub-cycle timescale. As a consequence, we expect the CEP to affect the harmonic dipole phases of the individual attosecond pulses in a different way: no CEP dependence of the dipole phase of the half-cycle plateau pulses (pulses 1 and 2 in figure 4(c)) versus a significant CEP dependence of the half-cycle cutoff pulse dipole phase (third pulse). This is confirmed by the observation of relative-phase variations with the

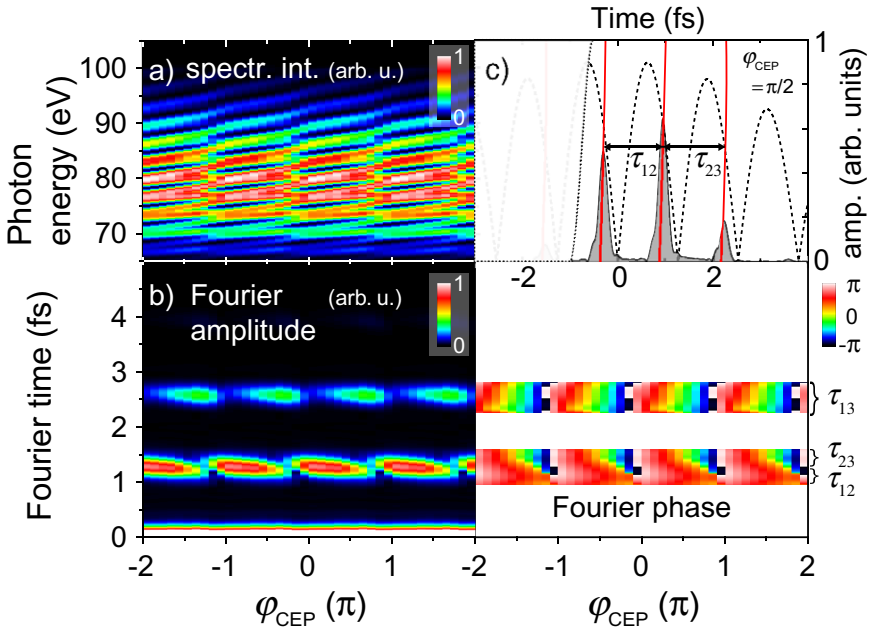

Figure 5. Same as figure 4 ((a), harmonic spectra versus CEP, (b) CEPSI analysis), but simulating time-dependent phase matching by plasma buildup, modeled by a temporal filter (indicated as the dotted line in (c)) and applied to the attosecond response from figure 4(c). The modulation and sloping of the CEPSI peak at Fourier time ∼2.5 fs observed experimentally in figure 2 are now also observed.

CEP only for the pulse delays τ_{nm} that contain the third pulse ($m = 3$). CEPSI thus allows the spectroscopic separation of the half-cycle plateau and cutoff region in the non-adiabatic regime of HHG. As a result, the dipole-phase CEP dependences of the half-cycle cutoff versus the half-cycle plateau energy region are directly retrieved in the experiment and measured here to change linearly by 2π per $\Delta\varphi_{CEP} = \pi$.

2.4. Possible effects of phase matching

The agreement between the experimental results (figure 2) and the quantum-mechanical model (figure 4) is nearly perfect in terms of the Fourier-phase behavior, which leads to the above-discussed spectroscopic separation of the half-cycle plateau and cutoff region. However, slight discrepancies remain, which are most pronounced in the Fourier amplitude. While the full-cycle Fourier peak in figure 2(b) slightly modulates in time as a function of φ_{CEP}, this modulation seems to be absent in the SFA results shown in figure 4(b). It is generally known [20] that phase matching modifies the single-atom response of HHG to arrive at the light field that is actually observed in experiments. The quantum-mechanical simulations so far implicitly include phase matching by only considering the short trajectory up to the cutoff region, which is expected when placing the harmonic generation cell downstream of the laser focus, as was done in the experiment.

In figure 5, we now discuss an aspect of phase matching, namely the temporal filtering of the XUV attosecond response, which is generally caused by a plasma buildup during the intense driving laser pulse. Phase matching is fully realized for a certain plasma density, and

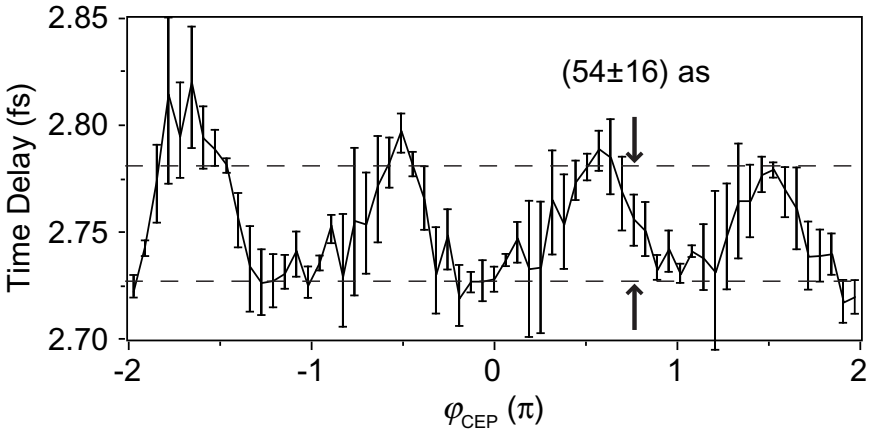

Figure 6. Mean time delay $\tau_{13} = \tau_{12} + \tau_{23}$ of the two outermost pulses in the attosecond-pulse triplet as a function of the CEP, extracted from the experimental results in figure 2. The error bars denote the standard deviation of the Gaussian fits to the π-periodic data sets. A fit to the systematic variation in time delay results in 54 ± 16 as (horizontal dashed lines) as the third pulse moves into and out of the cutoff region in the spectral range considered here (70–90 eV).

thus, for rather low laser intensities, typically leads to a cutting away of the leading edge, while at higher intensities the trailing edge will be cut off [11, 21, 22]. As we work at lower laser intensities here, we consider the case of cutting off attosecond pulses on the leading edge of the driver (figure 5(c)) by introducing a temporal filter. The resulting harmonic spectra are shown in figure 5(a). The corresponding CEPSI spectra (figure 5(b)) now reveal a further agreement with the experimental data shown in figure 2: the pronounced modulation and sloping of the CEPSI peak near Fourier time 2.5 fs.

This further improvement points out the remarkable sensitivity of CEPSI to minimal changes in the attosecond response, which will, in the future, lead to refined models of high-harmonic generation and improved physical understanding of strong-field processes in general.

2.5. Quantifying the relative timing of the attosecond pulses

Finally, as CEPSI separates individual sub-cycle contributions (temporally localized events) of the HHG spectrum, we now further use it to interferometrically quantify the CEP-dependent group delay between the two full-cycle spaced attosecond pulses in the experiment. The Fourier peak corresponding to $\tau_{13} = \tau_{12} + \tau_{23}$ in figure 2(b) is selected and fitted with a Gaussian function to determine its central position at each value of the CEP. The result is shown in figure 6, where a periodic modulation in time delay of 54 ± 16 as can be observed. An explanation for this modulation is as follows. For minimal group delays, the corresponding CEP values belong to situations where all three pulses contribute with their plateaus. In contrast, when the group delay is at its maximum, the corresponding attosecond-pulse configurations consist of only two pulses within their plateau region, while the third pulse on the trailing edge contributes with its own cutoff region (as indicated in figure 4(c)), resulting in a larger spacing τ_{13} between pulses 1 and 3. The apparent absence of this modulation in the single-atom SFA simulation shown in figure 4 is resolved by considering non-adiabatic phase matching, acting as an additional temporal gate as previously shown in figure 5.

3. Carrier–envelope phase-dependent electron photoemission from a nanoscale metal tip

To highlight the general applicability of the presented CEPSI method for strong-field physics and attosecond science, we apply the method to the recently observed coherent emission of photoelectrons from sharp metal tips driven by a few-cycle laser field [4, 23–28]. In our tip-based experiment [4, 28], we focus CEP-stable 6 fs pulses derived from a Ti:sapphire laser oscillator tightly on a nanoscale tungsten tip. Photoelectron spectra are recorded with an electron spectrometer. The light intensity at the tip is $\sim 1 \times 10^{13}\,\mathrm{W\,cm^{-2}}$ including the optical field enhancement effect [29]. Figure 7(a) shows the experimental results as previously published [4]. The figure presents the high-energy part of the spectrum where a rescattering plateau [30] is found. Varying the CEP strongly influences the shape of this spectral part and enables coherent control of electron wavepacket motion and matter–wave interference. The timing and occurrence of photoelectron bursts are controlled by the CEP with attosecond precision. Performing CEPSI analysis as described in the previous section reveals a number of characteristic temporal features that allow both additional physical (mechanistic) insight and a clear fingerprint for comparison to and validation of simulations (see below).

A CEP-dependent shift of the temporal delay between the photoelectron bursts emitted coherently from the metal tip can be immediately extracted from the CEPSI analysis. Furthermore, a phase shift of this emission with CEP is revealed, which closely follows the temporal shift. This indicates a constant relative phase of the two electron bursts irrespective of their temporal separation. Moreover, the presence of the temporal feature at 2.8 fs unambiguously shows that two attosecond wavepackets contribute to the photoelectron spectrum ('double slit in time'), whereas its absence at around $-0.3\pi < \varphi_{\mathrm{CEP}} < 0.3\pi$ indicates a single slit in time. As expected, subsequent bursts are separated by ~2.8 fs, which corresponds well to the optical cycle duration at a center wavelength of 800 nm (2.68 fs). Symmetry breaking at the tip's surface limits the occurrence of photoemission to every second half cycle in the pulse, contrary to what is known for atoms in the gas phase.

The experimental CEPSI spectrum can now be compared with the two different model simulations discussed in [4]. Both a semiclassical strong-field model (a) and the full numerical solution of a time-dependent Schrödinger equation (TDSE) model (b) were used to understand and evaluate the experimental results. Figure 8 shows the numerical results of these simulations after performing CEPSI analysis. The features discussed for the experimental CEPSI spectrum above now serve as a physically meaningful signature to evaluate the performance of the different models. The most striking characteristic is the temporal shifting with CEP of the ~2.8 fs Fourier-time feature that was observed in the experiment, and which is now absent in the strong-field model simulation. In comparison, the TDSE model clearly shows the expected CEP modulation of time delay and phase. The strong-field model shows two major differences from the TDSE model. Firstly, it neglects non-adiabatic electron dynamics, i.e. electron emission quasi-statically follows the laser electric field. Effects arising from non-adiabatic behavior, however, are expected for the experimental parameters of the measurement presented here (Keldysh parameter $\gamma \sim 2$). Secondly, in the simple strong-field model any electric-potential effects caused by the surface are neglected, such as the image force potential, which is explicitly taken into account in the TDSE model. This finding explicitly proves the sensitivity of coherent electron emission to the potential energy structure of the surface. Further experiments and comparison with more elaborate models such as time-dependent density-functional methods [30], aided by CEPSI analysis, will provide further

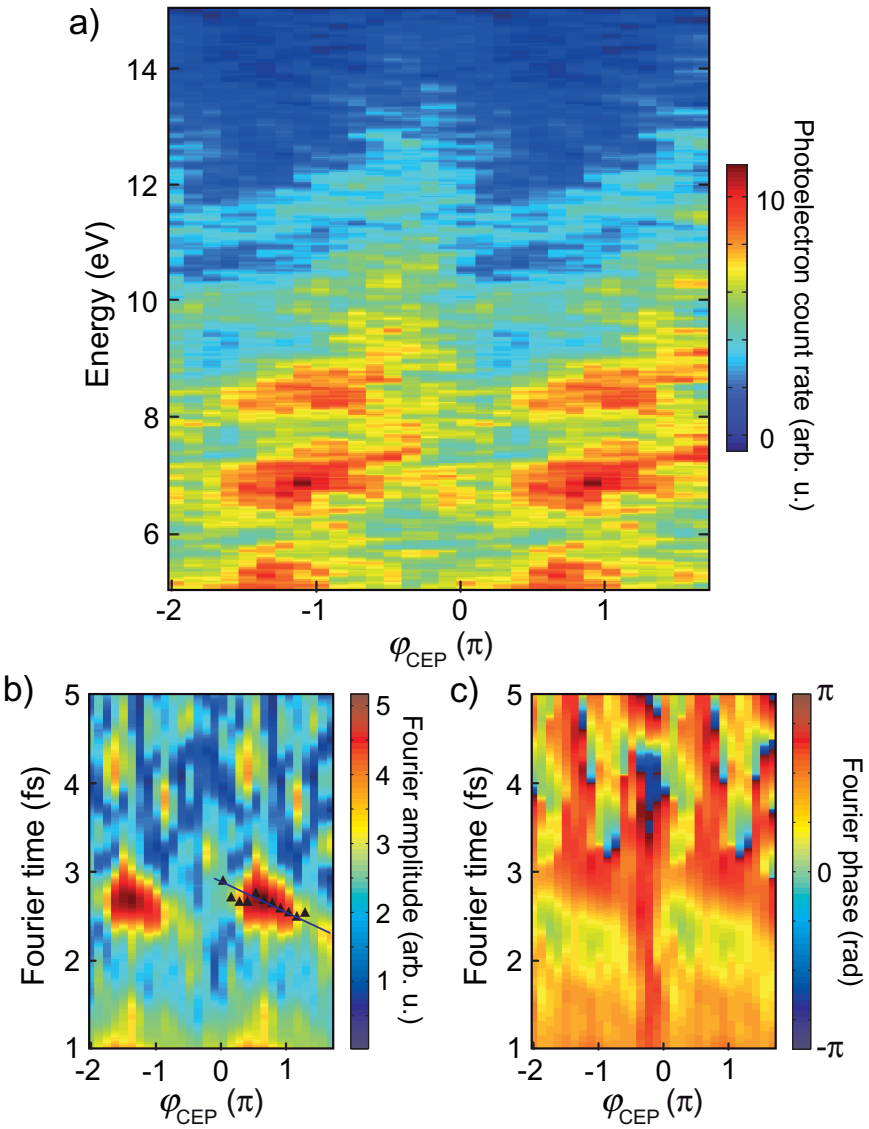

Figure 7. Experimental results for the CEP dependence of electron emission from sharp metal tips as discussed in [4]. (a) Original photoelectron data from the experiment. Only the plateau part is shown ($E > 5\,\mathrm{eV}$), where photoelectrons undergo rescattering. (b), (c) CEPSI analysis of the raw data, showing Fourier amplitude (b) and Fourier phase (c). The analysis reveals previously undiscovered temporal features of coherent electron emission from metal tips under laser irradiation: a shift of the temporal separation between two attosecond electron bursts versus CEP is apparent in (b) at a Fourier time around 2.8 fs. The black triangles indicate the center-of-mass position of a Gaussian fit to the amplitude peak, separately for each CEP value. A linear fit of these positions (blue line) indicates the trend. The separation varies from ∼2.9 to ∼2.5 fs, with a slope of $-(0.35 \pm 0.04)$ fs per π CEP. A similar shift is also observed in the Fourier phase shown in (c). Furthermore, the CEP regions for which only one attosecond wavepacket is expected ('single slit in time') are clearly identified in (b) by the absence of the temporal feature around 2.8 fs.

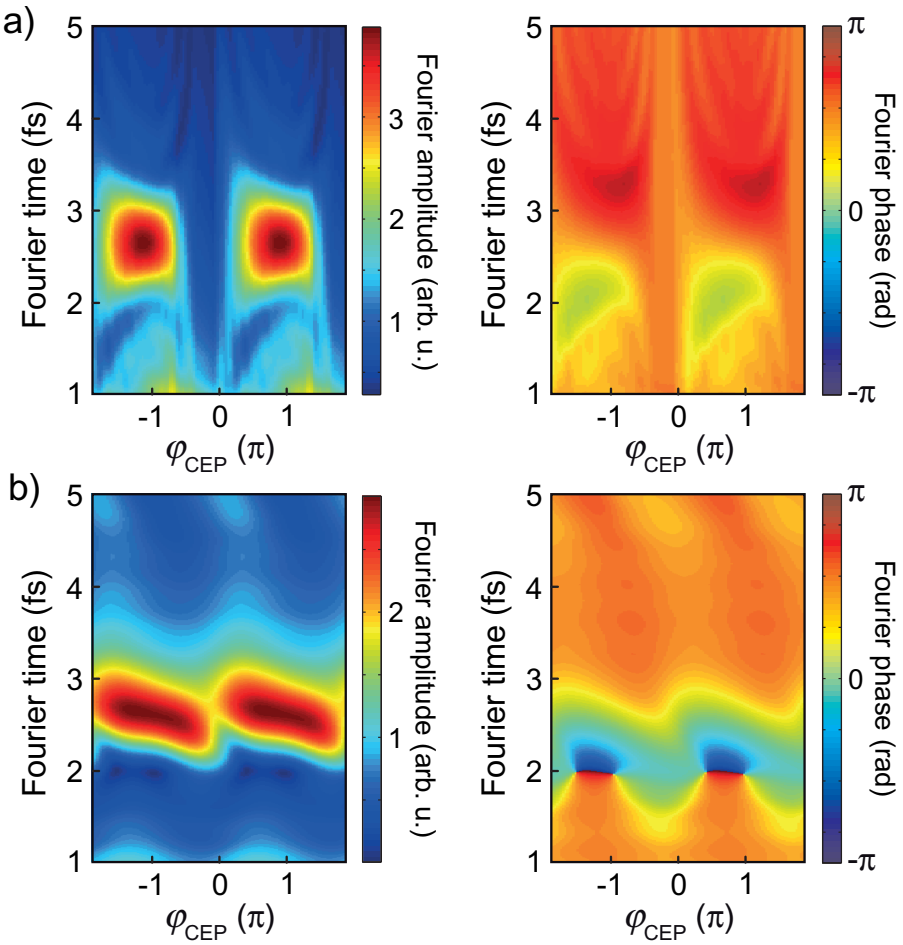

Figure 8. CEPSI analysis of the simulation results presented in [4]. (a) Quasi-classical strong-field trajectory simulation. (b) Full TDSE solution. A comparison of the strong-field model CEPSI plots to the experimental ones shows that the strong-field model does capture the double- versus single-slit behavior, but does not exhibit the CEP-dependent temporal shift. This point is nicely captured in the TDSE model. This implies the importance of non-adiabatic electron dynamics and/or of the electric-potential shape in the vicinity of the surface, both of which are absent in the strong-field model. Interestingly, the TDSE model does not exhibit the absence of interference around $\varphi \sim 0$ as clearly as in the experimental data, indicating that this model also possesses shortcomings.

evidence on the importance of surface fields, including induced polarization effects such as dynamical plasmons or nontrivially time-dependent image-charge phenomena.

4. Conclusion

In conclusion, we introduced the combination of CEP sweeping and SI, creating an attosecond sub-cycle 2D spectroscopy method to extract and quantify coherently interfering *temporally localized events* in strong-field processes. It allows us to separate temporally overlapping

coherent quantum paths, exhibiting a broad spectrum each, within the same strong-field driver pulse. The method is general and will enhance physical insight into many strong-field processes that are known to depend on the CEP within a single pulse. Further examples here are (above-threshold) ionization in the multiphoton or tunneling regime [31] and recollision physics in general, relativistic plasma dynamics [32] and electron localization in molecules [33]. In all these processes several different quantum (transition, transport, etc) pathways exist, with their phase depending sensitively on the CEP. CEPSI allows to disentangle the contributing quantum paths by mapping onto the essential representation in the time domain and thus to extract novel physical mechanisms as well as to quantify and test already existing ones with high (interferometric) temporal precision.

Acknowledgment

We are grateful to the Max-Planck Research Group program and the DFG (grant no. PF790/1-1) for funding.

References

[1] Udem T, Holzwarth R and Hänsch T W 2002 *Nature* **416** 233–7
[2] Baltuška A *et al* 2003 *Nature* **421** 611–5
[3] Lindner F, Schätzel M G, Walther H, Baltuška A, Goulielmakis E, Krausz F, Milošević D B, Bauer D, Becker W and Paulus G G 2005 *Phys. Rev. Lett.* **95** 040401
[4] Krüger M, Schenk M and Hommelhoff P 2011 *Nature* **475** 78–81
[5] Tokunaga E, Terasaki A and Kobayashi T 1992 *Opt. Lett.* **17** 1131–3
[6] Geindre J P, Audebert P, Rousse A, Falliès F, Gauthier J C, Mysyrowicz A, Santos A D, Hamoniaux G and Antonetti A 1994 *Opt. Lett.* **19** 1997–9
[7] Brixner T, Stenger J, Vaswani H M, Cho M, Blankenship R E and Fleming G R 2005 *Nature* **434** 625–8
[8] Engel G S, Calhoun T R, Read E L, Ahn T K, Mancal T, Cheng Y C, Blankenship R E and Fleming G R 2007 *Nature* **446** 782–6
[9] Salières P, Antoine P, de Bohan A and Lewenstein M 1998 *Phys. Rev. Lett.* **81** 5544–7
[10] Sansone G, Vozzi C, Stagira S and Nisoli M 2004 *Phys. Rev.* A **70** 013411
[11] Pfeifer T, Jullien A, Abel M J, Nagel P M, Gallmann L, Neumark D M and Leone S R 2007 *Opt. Express* **15** 17120–8
[12] Mansten E *et al* 2009 *Phys. Rev. Lett.* **102** 083002
[13] Antoine P, L'Huillier A and Lewenstein M 1996 *Phys. Rev. Lett.* **77** 1234–7
[14] Nisoli M, Sansone G, Stagira S, De Silvestri S, Vozzi C, Pascolini M, Poletto L, Villoresi P and Tondello G 2003 *Phys. Rev. Lett.* **91** 213905
[15] Abel M J, Pfeifer T, Jullien A, Nagel P M, Bell M J, Neumark D M and Leone S R 2009 *J. Phys. B: At. Mol. Opt. Phys.* **42** 075601
[16] Corkum P B 1993 *Phys. Rev. Lett.* **71** 1994–7
[17] Lewenstein M, Balcou P, Ivanov M Y, L'Huillier A and Corkum P B 1994 *Phys. Rev.* A **49** 2117–32
[18] Haworth C A, Chipperfield L E, Robinson J S, Knight P L, Marangos J P and Tisch J W G 2007 *Nature Phys.* **3** 52–7
[19] Balcou P, Dederichs A S, Gaarde M B and L'Huillier A 1999 *J. Phys. B: At. Mol. Opt. Phys.* **32** 2973–89
[20] Pfeifer T, Spielmann C and Gerber G 2006 *Rep. Prog. Phys.* **69** 443
[21] Jullien A, Pfeifer T, Abel M, Nagel P, Bell M, Neumark D and Leone S 2008 *Appl. Phys.* B **93** 433–42
[22] Abel M J, Pfeifer T, Nagel P M, Boutu W, Bell M J, Steiner C P, Neumark D M and Leone S R 2009 *Chem. Phys.* **366** 9–14

[23] Hommelhoff P, Sortais Y, Aghajani-Talesh A and Kasevich M A 2006 *Phys. Rev. Lett.* **96** 077401
[24] Hommelhoff P, Kealhofer C and Kasevich M A 2006 *Phys. Rev. Lett.* **97** 247402
[25] Ropers C, Solli D R, Schulz C P, Lienau C and Elsaesser T 2007 *Phys. Rev. Lett.* **98** 043907
[26] Barwick B, Corder C, Strohaber J, Chandler-Smith N, Uiterwaal C and Batelaan H 2007 *New J. Phys.* **9** 142
[27] Bormann R, Gulde M, Weismann A, Yalunin S V and Ropers C 2010 *Phys. Rev. Lett.* **105** 147601
[28] Schenk M, Krüger M and Hommelhoff P 2010 *Phys. Rev. Lett.* **105** 257601
[29] Martin Y C, Hamann H F and Wickramasinghe H K 2001 *J. Appl. Phys.* **89** 5774–8
[30] Wachter G, Lemell C, Burgdörfer J, Schenk M, Krüger M and Hommelhoff P 2012 *Phys. Rev.* B **86** 035402
[31] Paulus G G, Lindner F, Walther H, Baltuška A, Goulielmakis E, Lezius M and Krausz F 2003 *Phys. Rev. Lett.* **91** 253004
[32] Borot A, Malvache A, Chen X, Jullien A, Geindre J P, Audebert P, Mourou G, Quéré F and Lopez-Martens R 2012 *Nature Phys.* **8** 416–21
[33] Kling M F *et al* 2006 *Science* **312** 246–8